

1 **Development and Testing of a Novel Sulfur Dioxide Sonde**

2 Subin Yoon<sup>1</sup>, Alexander Kotsakis<sup>1,2</sup>, Sergio L. Alvarez<sup>1</sup>, Mark G. Spychala<sup>3,4</sup>, Elizabeth Klovenski<sup>1</sup>, Paul  
3 Walter<sup>3</sup>, Gary Morris<sup>3,5</sup>, Ernesto Corrales<sup>6</sup>, Alfredo Alan<sup>6</sup>, Jorge Andres Diaz<sup>6,7</sup>, James H. Flynn<sup>1</sup>

4 <sup>1</sup>Department of Earth and Atmospheric Sciences, University of Houston, Houston, TX, 77004, USA

5 <sup>2</sup>now at ERT, Inc., Laurel, MD, 20707, USA

6 <sup>3</sup>St. Edward's University, Austin, TX, 78704, USA

7 <sup>4</sup>now at Hamelmann Communications, Pagosa Springs, CO, 81147, USA

8 <sup>5</sup>now at NOAA Global Monitoring Laboratory, Boulder, CO, 80305, USA

9 <sup>6</sup>GasLAB, CICANUM. Universidad de Costa Rica, San José, Costa Rica

10 <sup>7</sup>now at INFICON, East Syracuse, NY, 13057, United States

11

12

13 *Correspondence to:* James H. Flynn (jhflynn@central.uh.edu)

14 **Abstract.** A novel technique has been developed to measure sulfur dioxide (SO<sub>2</sub>) using a modification of the existing  
15 electrochemical concentration cell (ECC) ozonesonde technology. The current sonde-based method to measure SO<sub>2</sub> (i.e., the  
16 dual-sonde approach) involves launching two ozonesondes together with one of the sondes having a filter to remove SO<sub>2</sub> at  
17 the inlet. The SO<sub>2</sub> profile is determined by taking the difference between the measurements from the two instruments. The  
18 dual-sonde method works well in typical tropospheric conditions when [O<sub>3</sub>] > [SO<sub>2</sub>] but saturates when [SO<sub>2</sub>] > [O<sub>3</sub>] and has  
19 large uncertainties in the upper troposphere/lower stratosphere that would limit its effectiveness in measuring SO<sub>2</sub> from an  
20 explosive volcanic eruption. Due to these limitations, several modifications were made to create a single-sonde system that  
21 would directly measure SO<sub>2</sub> (i.e., the SO<sub>2</sub> sonde). These modifications included (1) a positively biased ECC **background**  
22 current, (2) the addition of an O<sub>3</sub> removal filter, and (3) the addition of a sample dryer. The SO<sub>2</sub> sonde measures SO<sub>2</sub> as a  
23 reduction in the cell current. There was a strong correlation ( $r^2 > 0.94$ ) between the SO<sub>2</sub> sonde and a Thermo 43c analyzer  
24 during controlled laboratory tests and pre-flight tests. Varying humidity levels affected the SO<sub>2</sub> sonde's sensitivity ( $\text{avg} = 84.6$   
25  $\pm 31.7$  ppbv/ $\mu\text{A}$ ,  $1\sigma$  **RSD** = 37%) during initial field tests, which was resolved by adding a sample dryer upstream of the O<sub>3</sub>  
26 removal filter and pump inlet. This modification significantly reduced the variability and increased the sensitivity of the SO<sub>2</sub>  
27 measurements ( $\text{avg} = 47 \pm 5.8$  ppbv/ $\mu\text{A}$ ,  $1\sigma$  **RSD** = 12%). Field tests included measurements near Kilauea Volcano (before  
28 and during the 2018 eruption of the Lower East Rift Zone), Costa Rica's Turrialba Volcano, and anthropogenic plumes from  
29 the Athabasca Oil Sands region of Alberta, Canada. This single SO<sub>2</sub> sonde system is an effective, inexpensive instrument for  
30 measuring both ground-based and vertical profiles of SO<sub>2</sub> from anthropogenic and natural sources (i.e., volcanic eruptions)  
31 over a wide range of concentrations.

## 32 **1 Introduction**

33 Sulfur dioxide (SO<sub>2</sub>) emissions result from anthropogenic activities, such as power generation and crude oil refining processes,  
34 and natural sources, such as volcanoes. In gas form, SO<sub>2</sub> acts as a respiratory irritant leading to complications with asthma and  
35 cardiovascular conditions (Chen et al., 2007; Sunyer et al., 2003; Tzortziou et al., 2015, 2018). Gaseous SO<sub>2</sub> can be converted  
36 to sulfate aerosols (Zhang et al., 2015), which are highly scattering, reduce visibility, and can have a cooling effect on the  
37 **surface** climate when injected into the stratosphere (Kiehl and Briegleb, 1993; Schmidt et al., 2010). SO<sub>2</sub> acidifies rain,  
38 accelerating damage of infrastructure and vegetation, particularly near SO<sub>2</sub> sources such as volcanoes (Delmelle et al., 2002;  
39 Krug and Frink, 1983; Tortini et al., 2017). Due to these various climate, environmental, and human health-related impacts,  
40 anthropogenic SO<sub>2</sub> has been heavily monitored (Shannon, 1999; Zhang and Schreifels, 2011), and regulations have been  
41 enacted to reduce these emissions (EPA, 2000).

42  
43 The largest natural sources of SO<sub>2</sub> are volcanoes. The eruption of Mt. Pinatubo in the Philippines in June 1991 had global  
44 climatic effects and significant impacts on the tropospheric and lower stratospheric composition (Bluth et al., 1992; Parker et  
45 al., 1996). Apart from such catastrophic eruptions, SO<sub>2</sub> can be continually emitted from volcanoes. SO<sub>2</sub> plumes from over 90

46 volcanoes have been reliably detected by satellites, resulting in the injection of an estimated  $23 \pm 2 \text{ Tg yr}^{-1}$  of  $\text{SO}_2$  into the  
47 atmosphere (Carn et al., 2017). However, unlike anthropogenic sources of  $\text{SO}_2$ , most volcanoes lack routine ground monitoring  
48 (Galle et al., 2010; Pieri et al., 2013) and few opportunities exist for routine validation of satellite retrievals of  $\text{SO}_2$  with *in situ*  
49 measurements. ~~Small Unmanned-unmanned~~ aerial vehicle (UAV) platforms can measure volcanic plumes at altitudes of 2 km  
50 above the take-off altitude (Galle et al., 2010; Diaz et al., 2015); ~~while larger UAVs can measure stratospheric plumes (e.g.,~~  
51 ~~Global Hawk).~~ However, the lack and difficulty of monitoring and the possibility of another stratospheric injection of  $\text{SO}_2$   
52 motivated the development of an inexpensive but reliable balloon-borne instrument that could be deployed quickly after an  
53 eruption to validate satellite observations with *in situ* measurements.

54  
55 Radiosondes and ozonesondes have been widely used for measurements of various atmospheric parameters (e.g., temperature,  
56 air pressure, relative humidity [RH], and wind speed and direction) ~~and  $\text{O}_3$  concentrations~~, respectively. ~~These measurements~~  
57 ~~Electrochemical concentration cell (ECC) ozonesondes~~ produce vertical  $\text{O}_3$  profiles and allow for the validation of satellite  
58 based  $\text{O}_3$  vertical column density (VCD). ~~A schematic of the ECC is included in Figure S1.~~ The current sonde-based method  
59 for measuring  $\text{SO}_2$ , the dual-sonde method, uses two En-Sci (Environmental Science Inc., Westminster, CO) ~~ECC~~ ozonesondes  
60 in tandem (Morris et al., 2010). For the dual-sonde method, an  $\text{SO}_2$  removal filter is placed at the pump inlet of one of the  
61 ozonesondes, scrubbing  $\text{SO}_2$  from the sampled air before it enters the ~~electrochemical concentration cell (ECC)~~. The other  
62 sonde samples unfiltered air (i.e., air containing both  $\text{SO}_2$  and  $\text{O}_3$ ). Due to the chemical reactions in the cathode cell, the filtered  
63 sonde measures  $\text{O}_3$ , while the unfiltered sonde measures the difference between  $\text{O}_3$  and  $\text{SO}_2$  ( $[\text{O}_3] - [\text{SO}_2]$ ) since  $\text{SO}_2$  has an  
64 equal (relative to  $\text{O}_3$ ) but negative signal in the ECC (Morris et al., 2010). The  $\text{SO}_2$  concentrations are then determined from  
65 the difference between the two sonde measurements. This method works well in the troposphere when the  $\text{SO}_2$  concentration  
66 is less than the  $\text{O}_3$  concentration, but not as well in intense plumes, such as those found in eruptive volcanic environments.  
67 When the  $\text{SO}_2$  concentration exceeds the  $\text{O}_3$  concentration, the cell current in the unfiltered sonde becomes zero. The excess  
68  $\text{SO}_2$  saturates the dual-sonde and distorts the calculated  $\text{SO}_2$  profile. Additionally, in the stratosphere, where the  $\text{O}_3$  signal  
69 grows much larger than in the troposphere, the combined uncertainty of the measurements of the filtered and unfiltered sondes  
70 results in a large lower limit of detection (LLOD), on the order of tens of ppbv. Thus, a field deployment of the dual-sonde  
71 method more than a few days after an explosive, tropical volcanic eruption such as Mt. Pinatubo would result in little useful  
72 data in the critical upper troposphere/lower stratosphere region.

73  
74 This study reports on the development of a single instrument capable of *in situ*  $\text{SO}_2$  measurements in the presence or absence  
75 of  $\text{O}_3$ . This sonde can measure  $\text{SO}_2$  at much greater concentrations than  $\text{O}_3$  without saturating the system and can be configured  
76 for a sub-ppbv LLOD (calculated using  $3\sigma$ ) at sea level. Since  $\text{O}_3$  is removed from the sample stream, this  $\text{SO}_2$  sonde avoids  
77 the compounded ~~uncertainties/errors~~ of the dual-sonde method. Field deployments of the  $\text{SO}_2$  sonde include sampling of  
78 volcanic emissions from Kilauea on the Big Island of Hawai'i, U.S., Turrialba Volcano in Costa Rica, ~~and~~ the emissions from  
79 petroleum extraction and processing at the Athabasca Oil Sands, Canada. Results from these field tests, covering a wide range

80 of SO<sub>2</sub> concentrations from both natural and anthropogenic emission sources, are described below. The SO<sub>2</sub> sonde has been  
81 used for tethered and free-release balloons but can also be adapted for UAV platforms.

## 82 2 Instrumentation

### 83 2.1 Ozonesondes

84 The standard and modified ECC En-Sci ozonesondes were used for the O<sub>3</sub> and SO<sub>2</sub> sonde measurements in this study. The  
85 basic functioning of the ECC ozonesonde is described in Komhyr (1969) and Morris et al. (2010). The ECC sensor is composed  
86 of platinum cathode and anode electrodes, each in its own cell, immersed in a diluted and saturated solution of potassium  
87 iodide (KI), respectively. The cells are connected by an ion bridge allowing for the transfer of electrical charges while  
88 maintaining the separation of the solutions (Eq. 1 and 2). When the cells are charged with the solution, a transient potential  
89 difference is generated ~~that is but~~ dissipated through the redistribution of charge across the ion bridge. The following equilibria  
90 are established from these reactions:



93  
94 Sampled air is ~~diffused~~ pumped into the cathode cell, and the presence of O<sub>3</sub> initiates a reaction (Eq. 3) that causes an imbalance  
95 in favor of [I<sub>2</sub>] in the cathode solution.



97 To rebalance the ~~electrochemical potential of the~~ cell, the iodine/iodide redox reactions in ~~Eq. 4 and 5~~ result in a flow of  
98 electrons from the anode to the cathode via the ion bridge. This cell current, measured by an external ammeter, is proportional  
99 to the O<sub>3</sub> concentration.



102 ~~As is also described in in Komhyr (1969) and Morris et al. (2010), when-When~~ SO<sub>2</sub> is present in the sample air, an additional  
103 reaction (Eq. 6) occurs in the cathode cell of the ECC, supplying the two electrons needed to rebalance the cathode cell after  
104 the O<sub>3</sub> reaction (Eq. 3) (Komhyr, 1969; Morris et al., 2010).



106 Thus, each SO<sub>2</sub> molecule in the sampled air has the effect of cancelling the measurement of one O<sub>3</sub> molecule. In effect, the  
107 standard ECC ozonesonde reports [O<sub>3</sub>] - [SO<sub>2</sub>] for its measurement. In most places and at most times, [SO<sub>2</sub>] << [O<sub>3</sub>], so there

108 is not a significant impact on the O<sub>3</sub> measurements, but in places downwind of SO<sub>2</sub> sources (e.g., coal-burning power plants  
109 or volcanos), the O<sub>3</sub> measurement will be negatively impacted.

## 110 2.2 Instrumentation

111 Several SO<sub>2</sub> and O<sub>3</sub> instruments were used for validation of the SO<sub>2</sub> sonde during laboratory and field testing. A calibration  
112 system was used to produce controlled concentrations of SO<sub>2</sub> and O<sub>3</sub>. The calibration system relied on the operation of flow  
113 controllers or restrictors, an SO<sub>2</sub> ultra-high purity (UHP) gas cylinder (4.87 ppm; Scott-Marrin, Inc., Riverside, CA) and/or a  
114 U.V. Photometric O<sub>3</sub> calibrator (49C PS; Thermo Fisher Scientific, Franklin, MA), and zero air to produce desired pre-set  
115 concentration<sub>s</sub> of SO<sub>2</sub> and/or O<sub>3</sub>. The zero-air setup used for the field and laboratory testing was achieved using a dry zero air  
116 UHP gas cylinder or else generated by scrubbing ambient air through activated charcoal and Purafil SP (Purafil, Inc., Doraville,  
117 GA) canisters. The Thermo 43i-TL SO<sub>2</sub> analyzer (LLOD: 60-90 pptv at 5 min averaging) and the 49i O<sub>3</sub> analyzer (LLOD: 1.5  
118 ppbv at 5 min averaging) were also used during laboratory testing, while a Thermo 43c-TL SO<sub>2</sub> analyzer was used during field  
119 testing in Hawai'i. These instruments were set to report 10 s average measurements.

## 120 3 Single-sonde SO<sub>2</sub> System and Laboratory Testing

### 121 3.1 SO<sub>2</sub> sonde system description

122 ~~The single-sonde~~ ~~The first version (version 1.0) of the single-sonde~~ SO<sub>2</sub> system (i.e. SO<sub>2</sub>-sonde v1.0) included ~~threetwo~~ major  
123 modifications to the En-Sci ECC ozonesonde: (1) the application of a positively biased ~~baekground~~-current to the cathode cell,  
124 ~~and~~ (2) the addition of an O<sub>3</sub> removal filter, ~~and~~ (3) a sample dryer (Fig. S1). ~~The first version of the SO<sub>2</sub> system (SO<sub>2</sub> sonde~~  
125 ~~v1.0) included the first two modifications: the bias current and an O<sub>3</sub> removal filter. The bias current sets the upper limit of~~  
126 ~~detection (ULOD) for the SO<sub>2</sub> sonde and is set prior to measurement. The O<sub>3</sub> removal filter is placed in line with the inlet~~  
127 ~~allowing O<sub>3</sub>-free air to be sampled in the SO<sub>2</sub> sonde. In a standard~~the ECC, O<sub>3</sub> produces a positive response signal while SO<sub>2</sub>  
128 produces a negative signal when sufficient O<sub>3</sub> ~~is present~~ (i.e., positive signal) ~~is present~~. With these ~~two~~ modifications, SO<sub>2</sub>  
129 can be measured directly as the reduction of the cell current from the pre-set biased ~~baekground~~-current (Flynn and Morris,  
130 2021). Unlike the dual-sonde system, this approach allows for direct SO<sub>2</sub> measurements rather than an inference by subtraction  
131 of signals from two separate instruments. ~~A sample dryer was added to the SO<sub>2</sub> sonde in the second version (v1.1) to combat~~  
132 ~~humidity issues discovered after initial field tests. The addition of the dryer corrected the highly varying instrument sensitivity~~  
133 ~~observed in the field.~~ All components of the SO<sub>2</sub> sonde fit within a standard ozonesonde foam box (approximately 8" x 8" x  
134 10") except for the inlet filter. The free-release balloon payload's total mass is approximately 1 kg. The patent publication ~~and~~  
135 ~~Fig. S1~~ provides a detailed description and schematic of the SO<sub>2</sub> sonde (Flynn and Morris, 2021).

Formatted: Subscript

Formatted: Subscript

Formatted: Subscript

Formatted: Subscript

Formatted: Subscript

### 3.2 Testing of ~~background-the bias~~ current

The ~~background~~-bias current is supplied by inserting into the cathode cell an additional platinum electrode ~~in the cathode cell~~ powered by a 9V battery (Fig. S1) (Flynn and Morris, 2021). To maintain consistent power, the circuit uses a 5V regulator.

Varying the ~~resistor~~resistance allows for a range of bias currents to be introduced. The current version of the SO<sub>2</sub> sonde uses a fixed resistor which requires a priori knowledge of the desired SO<sub>2</sub> concentration range. The desired resistor is installed in series with the battery and the electrode ~~allows for a range of bias currents to be introduced~~. An earlier Laboratory-laboratory

tests compared the SO<sub>2</sub> sonde measurements (initially configured without an O<sub>3</sub> removal filter) to those made by a 43i-TL SO<sub>2</sub> analyzer (Fig. 1, Table 1). O<sub>3</sub> and SO<sub>2</sub> gases were introduced using the laboratory calibration setup and a manifold to allow the sonde and the Thermo trace gas instruments to sample the same air. Results in Fig. 1 show 60 s averaged data. The test included (A) input of O<sub>3</sub> without an added ~~background-bias~~ current; (B) the same input of O<sub>3</sub> with the addition of a ~~background~~

~~bias~~ current (equivalent to ~~a signal of~~ approximately 90 ppbv of O<sub>3</sub>); and the addition of SO<sub>2</sub> to the O<sub>3</sub> with the enhanced ~~background-bias~~ signal where the SO<sub>2</sub> concentration was either (C) smaller or (D ~~and~~– E) larger than the O<sub>3</sub> concentration.

During (A), measurements made by O<sub>3</sub> and SO<sub>2</sub> sondes compare well to measurements made by the Thermo instruments (Fig.1, Table 1). The test included (E) the response of the SO<sub>2</sub> sonde to with a stepwise reduction of the O<sub>3</sub> concentration resulting in an equivalent decrease in signal, followed by (G – I) a stepwise reduction in the SO<sub>2</sub> concentration resulting in an equivalent increase in signal. At (F), the SO<sub>2</sub> concentration exceeded the ~~biased background~~ current (90 ppbv), producing a signal equivalent to  $2.9 \pm 0.1$  ppbv, resulting in no sonde response. ~~During the full test,~~ The sonde successfully measured SO<sub>2</sub> both with and without O<sub>3</sub> with approximately 97.97% efficiency.

Examination of the SO<sub>2</sub> sonde data showed that noise was proportional to the measured signal, with 1- $\sigma$  noise at approximately 0.2 – 0.3% of the measured signal. Because increases in the SO<sub>2</sub> concentration s result in ~~a~~ decreases in the signal (i.e., lower cell currents), the magnitude of the applied ~~background-current~~-bias current determines the saturation point (i.e., ~~upper limit of detection~~ {ULOD}) of the SO<sub>2</sub> sonde; saturation occurs when the measured cell current drops to zero. Applying a higher ~~background-bias~~ current increases the ULOD but also increases noise and the LLOD. The reported LLODs of bias currents are calculated as  $3\sigma$  relative to the baseline signal when sampling zero air. During laboratory testing, the LLOD ( $3\sigma$ ) was calculated for a range of applied ~~background-current~~-bias currents (0.25 to 10.0  $\mu$ A). The LLOD for the varying bias current of 0.25 to 10.0  $\mu$ A ranged from approximately 0.002 to 0.084  $\mu$ A, respectively. Results of calculated LLOD of a 0.25  $\mu$ A bias current at varying replicated altitudes is included in Table S1. At the surface, the LLOD of 20s averaged measurements is 0.17 ppbv.

The final version of the SO<sub>2</sub> sonde (v1.1) requires the bias current to be selected prior to measurement. If the bias current is set too low, a measurement of larger than expected SO<sub>2</sub> concentrations can saturate the sensor while a bias current that is set too high will have higher LLOD due to the increase in noise. The applied magnitude of the bias current can be best determined based on known SO<sub>2</sub> sources including volcanic emissions, urban and/or industrial emissions.

Formatted: Subscript

Formatted: Subscript

Formatted: Subscript

Formatted: Subscript

Formatted: Subscript

### 3.3 Testing of O<sub>3</sub> removal filter

Since the ECC responds to both O<sub>3</sub> and SO<sub>2</sub>, an O<sub>3</sub> removal filter was developed to remove interference from O<sub>3</sub> in the sample. This proprietary O<sub>3</sub> removal filter is placed upstream of the sonde inlet (Flynn and Morris, 2021). During laboratory testing, the O<sub>3</sub> removal filter was exposed to a continual concentration of  $487 \pm 3$  ppbv of O<sub>3</sub> and a varying concentration of SO<sub>2</sub> ranging from 0 to  $111 \pm 1$  ppbv (Fig. 2). The O<sub>3</sub> was effectively and consistently removed from the sampled air by the O<sub>3</sub> removal filter ~~as during a stepwise dilution of~~ SO<sub>2</sub> ~~was diluted~~. The testing included measurements with (~~white-gray~~ background) and without (~~gray-white~~ background) the O<sub>3</sub> removal filter. The SO<sub>2</sub> and O<sub>3</sub> concentrations measured by the Thermo 43i-TL and 49i instruments, respectively, and changes in SO<sub>2</sub> dilution levels are also indicated in Fig. 2. The O<sub>3</sub> removal filter destroyed the O<sub>3</sub> at all SO<sub>2</sub> dilution levels to below the detection limit of the O<sub>3</sub> instrument. By comparing the Thermo 43i-TL SO<sub>2</sub> analyzer measurements with and without the O<sub>3</sub> removal filter, SO<sub>2</sub> passed through the filter with 88% efficiency (Fig. ~~S1a3a~~). The transmission efficiency was calculated by taking the ratio of SO<sub>2</sub> measured by the sonde to ~~that~~ ~~measured by~~ the analyzer. The SO<sub>2</sub> transmission efficiency increased to 97% when testing the O<sub>3</sub> removal filter with the dry zero air UHP gas cylinder (Fig. ~~S1b3b~~) instead of the ~~zero air/zero-air~~ generator that processes ambient laboratory air (Fig. ~~S1a3a~~). Additional testing of the O<sub>3</sub> removal filter demonstrated that the filter removed approximately 1 ppm of O<sub>3</sub> at sea level with > 99.9% ~~in O<sub>3</sub> removal~~ efficiency, ~~concentrations~~ below the detection limit of the Thermo 49i O<sub>3</sub> monitor.

### 3.4 Sample Dryer

~~The SO<sub>2</sub> sonde v1.0 had highly varying sensitivities during the initial field tests. The instrument sensitivity was determined by regression analysis of the sonde's cell current to the SO<sub>2</sub> concentration measured by an SO<sub>2</sub> analyzer. The variability in the sensitivities was hypothesized to be due to differing levels of humidity during each SO<sub>2</sub> sonde launch. SO<sub>2</sub> is soluble in water and through multiphase reactions can be oxidized to sulfuric acid in the atmosphere in the presence of water vapor (e.g., precipitation, clouds, fog, etc.) (Carmichael and Peters, 1979; Zhang et al., 2013; Terraglio and Manganelli, 1967). Factors including liquid water content, aerosol composition, aerosol loading, and pH of the water are important in determining the adsorption and oxidation rates of SO<sub>2</sub> (Liu et al., 2021). When air with elevated humidity is flowing through a filter, SO<sub>2</sub> gas is likely adsorbing on the filter causing lower SO<sub>2</sub> transmission efficiency due to the potential uptake of SO<sub>2</sub> in water on the filter. Several laboratory tests confirmed the need to remove water from the sample upstream of the O<sub>3</sub> removal filter to improve the measurement of SO<sub>2</sub>. A desiccant membrane dryer (Perma Pure LLC, Lakewood, NJ) composed of a Nafion™ tube in silica gel desiccant was placed in-line upstream of the O<sub>3</sub> removal filter. This sample dryer is lightweight, relatively inexpensive, and does not require power.~~

Laboratory tests included exposing the SO<sub>2</sub> sonde, with and without a sample dryer, to controlled levels of humidity and SO<sub>2</sub>. Without removing water vapor, the SO<sub>2</sub> transmission efficiency decreases as humidity increases, particularly above 50% RH (Fig. 6). As the O<sub>3</sub> removal filter is humidified, the SO<sub>2</sub> transmission efficiency decreases. With the sample dryer in place,

Formatted: Subscript

200 each of the laboratory SO<sub>2</sub> transmission efficiency (May 17-18 and 21, 2018) tests varied by an average of <1% across a range  
201 of 0-85% RH (Fig. 6).

202  
203 The dryer's useful lifetime was determined by continuously exposing it to high humidity (> 95% RH at approximately 23 °C)  
204 sample stream. The downstream RH climbed from 5% to 16% after 2.3 h and to 25% after 6.3 h. At these downstream RH  
205 levels, the SO<sub>2</sub> transmission efficiency remained above 95%. A typical SO<sub>2</sub> sonde's measurement time per flight, including  
206 pre-flight calibration, is approximately three hours. The dryer's useful lifetime is likely much longer than required for a balloon  
207 flight since exposure to 95% RH conditions for several hours is highly unusual outside of hurricanes and tropical systems. SO<sub>2</sub>  
208 sonde and Thermo 43c-TL measurements were strongly correlated ( $r^2 = 0.99$ ) during a multipoint calibration conducted using  
209 the O<sub>3</sub> removal filter and the dryer under relatively high humidity levels. During that calibration, the SO<sub>2</sub> sonde's sensitivity  
210 was  $45.43 \pm 0.17$  ppbv/ $\mu$ A. By comparison, the average sensitivity during the initial Hawaii deployment was  $84.6 \pm 31.7$   
211 ppbv/ $\mu$ A across 10 sondes. The sample dryer, therefore, improved both the sensitivity and stability of the measurements  
212 observed. The addition of the sample dryer is necessary for providing accurate ambient SO<sub>2</sub> measurements.

#### 213 214 **4. Field Deployments, Part I with SO<sub>2</sub> sonde v1.0**

215 The ~~is~~ SO<sub>2</sub> sonde (SO<sub>2</sub> sonde v1.0), ~~single-SO<sub>2</sub> sonde without the sample dryer~~, was deployed and tested in Hawai'i and Costa  
216 Rica (Fig. S2). The field sites were close to active volcanoes, which are significant sources of natural SO<sub>2</sub> (Tang et al., 2020;  
217 Carn et al., 2017). In Hawai'i, field measurements were made near Kīlauea Volcano on the south-eastern shore of Island of  
218 Hawai'i, the largest of Hawai'i's islands. Kīlauea is the youngest volcano on the island and one of Earth's most active volcanoes  
219 (Kern et al., 2015; Nadeau et al., 2015). Kīlauea had been in a state of eruption since 1983 (Patrick et al., 2019) with an average  
220 SO<sub>2</sub> release rate of approximately 5,500 T/d measured during 2014 – 2017 (Elias et al., 2018). In Costa Rica, field  
221 measurements were made near Turrialba Volcano, one of the most active volcanoes in the Central American Volcanic Arc.  
222 Studies of emissions from Turrialba prior to 2013 reported SO<sub>2</sub> release rates of up to 4,000 T/d (de Moor et al., 2016; Xi et al.,  
223 2016). ~~The Activity activity escalated of Turrialba increased~~ after 2014, raising concerns for air quality and environmental  
224 health (de Moor et al., 2016; Tortini et al., 2017).

#### 225 **4.1 Kīlauea, Hawai'i - February 2018**

226 The first deployment of the SO<sub>2</sub> sonde v1.0 was during NASA's HypsIRI HyTES Hawaii Campaign (H3C) from February 3-  
227 10, 2018, near Kīlauea Volcano. The instrument was tested in flights on free-release balloons and a tethered balloon system  
228 (TBS), and at ground level with measurements in Hawaii Volcanoes National Park (HVNP) downwind of Kīlauea's summit  
229 crater, Halema'uma'u. During the ground-level testing, an SO<sub>2</sub> sonde and a Thermo 43c-TL SO<sub>2</sub> analyzer's sample inlet were  
230 mounted on the top of a van for co-located sampling.

Formatted: Normal

Formatted: Subscript

Formatted: Subscript



231 Figure 3a-4a depicts the measurements taken during the first encounter with an SO<sub>2</sub> plume while driving through the HVNP  
232 on February 3, 2018. The strongly correlated SO<sub>2</sub> sonde and Thermo 43c-TL measurements ( $r^2 = 0.99$ ) reached upward of  
233 ~940 ppbv. The SO<sub>2</sub> sonde had a sensitivity of  $118.4 \pm 0.4$  ppbv/ $\mu$ A, determined by regression analysis of the sonde's cell  
234 current with the Thermo 43c-TL concentrations (Fig. 3a4a). The SO<sub>2</sub> sonde sensitivity varied significantly during the field  
235 deployment. During surface measurements on February 10, 2018, earlier zero-air calibrations measured a sensitivity of  $86.5 \pm$   
236  $1.5$  ppbv/ $\mu$ A, while measurements during an SO<sub>2</sub> plume event, with peak concentrations of up to 400 ppbv, found the SO<sub>2</sub>  
237 sonde's sensitivity was  $73.9 \pm 0.6$  ppbv/ $\mu$ A (Fig. 3b4b). Although the SO<sub>2</sub> sonde sensitivity varied significantly in ten  
238 subsequent calibrations ( $84.6 \pm 31.7$  ppbv/ $\mu$ A), the measurements remained strongly correlated (range:  $r^2 = 0.94 - 0.99$ ). The  
239 variability in the sensitivity in the field was likely due to changes in the ambient RH impacting the SO<sub>2</sub> transmission efficiency  
240 of the O<sub>3</sub> removal filter. This hypothesis was further confirmed by laboratory RH testing and discussed in Sect. 3.3 and 3.4.

#### 241 4.2 Turrialba, Costa Rica (Dual-sonde versus SO<sub>2</sub> sonde comparison)

242 On March 23, 2018, ~~the University of Houston/St. Edward's University team conducted a traditional SO<sub>2</sub> dual-sonde payload~~  
243 ~~(Morris et al., 2010) as well as the SO<sub>2</sub> sonde v1.0 were launched using a free-release balloon~~ flight from the Universidad de  
244 Costa Rica's campus in San Jose (approximately 31 km downwind of Turrialba Volcano) ~~consisting of a traditional SO<sub>2</sub> dual-~~  
245 ~~sonde payload (Morris et al., 2010) as well as the SO<sub>2</sub> sonde v1.0.~~ This flight provided the first direct *in situ* comparison of the  
246 two SO<sub>2</sub> sonde methods. Figure 4-5 shows the response of the SO<sub>2</sub> sonde v1.0 and the calculated SO<sub>2</sub> dual-sonde profile. The  
247 dual-sonde SO<sub>2</sub> method can only report concentrations of SO<sub>2</sub> up to a maximum of the concentration of O<sub>3</sub> present.  
248 Furthermore, because the SO<sub>2</sub> concentration is determined by subtracting the signals from two instruments, its uncertainty is  
249 higher than the uncertainty of a measurement from a single instrument. When  $[\text{SO}_2] > [\text{O}_3]$ , the dual sonde's unfiltered  
250 ozonesonde signal goes to zero, as happened for the Turrialba sonde launch between 3 – 5 km (Fig. 45). The SO<sub>2</sub> saturates the  
251 cathode solution in the unfiltered sonde, not recovering until enough ambient O<sub>3</sub> has been processed to rebalance the cell,  
252 resulting in a distorted profile (Fig. 45). For this flight, the SO<sub>2</sub> sonde was configured to its maximum range (ULOD of  
253 approximately 450 ppbv at standard pressure) and was able to capture both the small plume below 2 km above mean sea level  
254 (AMSL) (approximately 18 ppbv) as well as the primary plume between 3 – 4 km AMSL (approximately 230 ppbv). The SO<sub>2</sub>  
255 sonde v1.0 was able to capture the full shape of the profile, including the peak values and structure of the plume. The SO<sub>2</sub>  
256 sonde v1.0 reports the top of the plume around 4 km AMSL, whereas the dual-sonde remains saturated until closer to 5 km  
257 AMSL. Thus, the dual-sonde SO<sub>2</sub> profiles, when saturated by high concentrations of SO<sub>2</sub>, erroneously appear to have a greater  
258 vertical extent. Further, the SO<sub>2</sub> sonde v1.0 showed no interference from O<sub>3</sub> at altitudes from the surface to altitude at 24.4 km  
259 AMSL, with O<sub>3</sub> concentrations in the stratospheric O<sub>3</sub> layer reaching  $> 4$  ppmv (not shown), demonstrating the effectiveness  
260 of the O<sub>3</sub> filter. The SO<sub>2</sub> VCD was 8.3 DU (Dobson Units, 1 DU =  $2.69 \times 10^{16}$  molecules  $\text{cm}^{-2}$ ) for the SO<sub>2</sub> sonde but was only  
261 3.4 DU for the dual-sonde measurement. Thus, once saturated, the dual-sonde method may is likely to underestimate the SO<sub>2</sub>  
262 VCD. Additional laboratory testing is planned to resolve this discrepancy.

#### 263 5. Post-Field-Test Improvements and Laboratory Testing

Formatted: Normal

264 The variability in the SO<sub>2</sub> sonde v1.0's sensitivity during the initial field tests was hypothesized to be due to varying levels of  
265 humidity. SO<sub>2</sub> is soluble in water and through multiphase reactions can be oxidized to sulfuric acid in the atmosphere in the  
266 presence of water vapor (e.g. precipitation, clouds, fog, etc.) (Carmichael and Peters, 1979; Zhang et al., 2013; Terraglio and  
267 Manganelli, 1967). Factors including liquid water content, aerosol composition, aerosol loading, and pH of the water are  
268 important in determining adsorption and oxidation rate of SO<sub>2</sub> (Liu et al., 2021). With increased humidity and presence of a  
269 filter, SO<sub>2</sub> gas is likely adsorbing on the filter causing lower SO<sub>2</sub> transmission efficiency due to potential uptake of SO<sub>2</sub> in  
270 water on the filter. Several laboratory tests were done to confirm the need to remove water from the sample upstream of the  
271 O<sub>3</sub> removal filter. A desiccant membrane dryer (Perma Pure LLC, Lakewood, NJ) composed of a Nafion<sup>TM</sup> tube in silica gel  
272 desiccant was placed in line upstream of the O<sub>3</sub> removal filter. This sample dryer is lightweight, relatively inexpensive, and  
273 does not require power.

274  
275 Laboratory tests included exposing the SO<sub>2</sub> sonde, with and without a sample dryer, to controlled levels of humidity and SO<sub>2</sub>.  
276 Without removing water vapor, the SO<sub>2</sub> transmission efficiency decreases as humidity increases, particularly above 50% RH  
277 (Fig. 5). As the O<sub>3</sub> removal filter is humidified, the SO<sub>2</sub> transmission efficiency decreases due to increased SO<sub>2</sub> loss in the  
278 filter. With the sample dryer in place, the SO<sub>2</sub> transmission efficiency varies by an average of <1% across a range of 0-85%  
279 RH (Fig. 5).

280  
281 The dryer's useful lifetime was determined by continuously exposing it to high humidity (> 95% RH at approximately 23 °C)  
282 sample stream. The downstream RH climbed from 5% to 16% after 2.3 h and to 25% after 6.3 h. At these downstream RH  
283 levels, the SO<sub>2</sub> transmission efficiency remained above 95%. A typical SO<sub>2</sub> sonde's measurement time per flight, including  
284 pre-flight calibration, is approximately three hours. The dryer's useful lifetime is likely much longer than required for a flight  
285 since exposure to 95% RH conditions for several hours is highly unusual outside of hurricanes and tropical systems for balloon  
286 measurements. SO<sub>2</sub> sonde and Thermo 43c TL measurements were strongly correlated ( $r^2 = 0.99$ ) during a multipoint  
287 calibration conducted using the O<sub>3</sub> removal filter and the dryer under relatively high humidity levels. During that calibration,  
288 the SO<sub>2</sub> sonde's sensitivity was  $45.43 \pm 0.17$  ppbv/ $\mu$ A. By comparison, the average sensitivity during the H3C campaign was  
289  $84.6 \pm 31.7$  ppbv/ $\mu$ A across 10 sondes. The sample dryer, therefore, improved both the sensitivity and stability of the  
290 measurements observed.

## 291 **6.5 Field Deployments, with SO<sub>2</sub> Sonde v1.1Part II**

292 The updated SO<sub>2</sub> sonde (SO<sub>2</sub> sonde v1.1) with the dryer filter was deployed and tested in near Ft. McMurray Mackay, Canada,  
293 and again in Hawai'i in June 2018. Ft. McMurray Mackay is in the Alberta province of Canada and is home to the Athabasca  
294 Oil Sands, a large area of bitumen and heavy crude oil surface deposits high in sulfur content. Local processing of these  
295 products (e.g., surface mining) and resulting by-products (e.g., tailing ponds) can release significant amounts of SO<sub>2</sub> into the

Formatted: Subscript

296 atmosphere (Bari et al., 2020; McLinden et al., 2016; Simpson et al., 2010). A second field deployment to Hawai'i followed  
297 immediately after the deployment to Canada. On May 3, 2018, Kīlauea Volcano on Hawai'i entered a new eruptive phase with  
298 an outbreak of a series of fissures in the lower Puna area (Liu et al., 2021; Anderson et al., 2019; Gansecki et al., 2019; Patrick  
299 et al., 2020). The active phase volcanic gas emissions resulted in localized evacuations in the Lower East Rift Zone (LERZ),  
300 ~~destroying more than 700 homes and displacing thousands of residents~~, and ~~resulting in~~ poor air quality for much of the  
301 southern and western portions of the island (Tang et al., 2020). The eruption event entered a paused phase in early August, and  
302 was declared over on December 5, 2018 (Kern et al., 2020).

### 303 **6.5.1 Athabasca Oil Sands, Canada**

304 The SO<sub>2</sub> sonde v1.1 was tested in Ft. ~~MaeKay-Mackay~~ (near Ft. McMurray; 57.1206° N, 111.4241° W), Alberta, in the  
305 Athabasca Oil Sands from June 10 – 16, 2018 (Fig. S2c). This field project, conducted in conjunction with Environment  
306 Canada and York University, evaluated SO<sub>2</sub> emissions from industrial activities in and near the oil sands region using a  
307 combination of TBS and ground-based measurements. The SO<sub>2</sub> sonde v1.1 was flown on the York TBS payload recording  
308 measurements from the ground to 300 m above ground level (AGL; 650 m AMSL). This deployment provided a dilute  
309 anthropogenic plume to test the SO<sub>2</sub> sonde in a high-sensitivity, low-range configuration. The average sensitivity of the SO<sub>2</sub>  
310 sonde v1.1 during the project was 51 ± 1.2 ppbv/μA. The SO<sub>2</sub> sonde was configured to sample in a range from ~0.5-25 ppbv  
311 of SO<sub>2</sub>. The TBS SO<sub>2</sub> sonde's vertical profiles were averaged into 10 m altitude bins that measured SO<sub>2</sub> concentration ranges  
312 that are more representative of anthropogenically-impacted SO<sub>2</sub> rather than large volcanic plumes (Fig. 67). This field  
313 deployment also demonstrated the performance of the sonde at sub-ppbv levels of ambient SO<sub>2</sub>.

### 314 **6.5.2 Kīlauea, Hawai'i - June 2018**

315 In response to the larger eruption that started in May 2018, the SO<sub>2</sub> sonde v1.1 was deployed to Hawai'i for the NASA-funded  
316 Big Island SO<sub>2</sub> Survey (BISOS). The SO<sub>2</sub> sonde launches occurred from Kahuku Ranch (19.0549° N, 155.6934° W) and  
317 Na'alehu Elementary School (19.0610° N, 155.5788° W) approximately 90 km downwind of Kīlauea's LERZ (Fig. S2d). The  
318 site's distance from the source allowed the plume to disperse and dilute as compared with measurements at the vent. An SO<sub>2</sub>  
319 plume was detected during seven of the nine free-release balloon launches during the June 2018 BISOS campaign. The ten  
320 SO<sub>2</sub> sonde v1.1 calibrations performed during BISOS had an SO<sub>2</sub> sensitivity of 47.0 ± 5.8 ppbv/μA and were similar to the  
321 laboratory results ~~using dry air~~ (45.43 ± 0.17 ppbv/μA).  
322

323 With the anticipated levels of SO<sub>2</sub>, the sondes were configured to sample ~~in the~~at the maximum range of 10-450 ppbv of  
324 SO<sub>2</sub>. Figure 7-8 shows four distinctive SO<sub>2</sub> profiles, and Table 2 includes the VCDs for each flight. No plumes above 5 km  
325 AMSL were detected, ~~at which point reductions in air density significantly impacted the LLOD~~. All but one of the observed  
326 SO<sub>2</sub> plumes were below the capping inversion of the planetary boundary layer (PBL). On June 22 (Fig. 7a8a), the ascent  
327 profile shows SO<sub>2</sub> below 3 km AMSL peaking at nearly 100 ppbv and additional features between 3-4 km AMSL peaking at

328 20–35 ppbv (Tang et al., 2020). The latter peaks were correlated with higher RH, perhaps the result of steam from a vent or  
329 the ocean entry points having broken through the inversion. The early afternoon June 28 profile (Fig. 7b8b) shows the  
330 highest concentration (325 ppbv) for a resolved SO<sub>2</sub> plume during the BISOS campaign. Typical for the trade winds, NOAA  
331 HYSPLIT trajectories (Stein et al., 2015) showed the winds were out of the NE, consistent with the plume’s transport from  
332 vents in the LERZ or the lava ocean entry points. Although the descent profile from a June 29 early afternoon launch lost the  
333 signal at 0.58 km AMSL, Fig. 7e-8c shows an SO<sub>2</sub> plume over the ocean with a peak concentration of 188 ppbv at 0.74 km  
334 AMSL. HYSPLIT trajectories again showed the winds were out of the NE. Lastly, the SO<sub>2</sub> plume detected during the ascent  
335 of the June 30 launch (Fig. 87d) exceeded the ULOD between 1–3 km AMSL for the SO<sub>2</sub> sonde configuration used. The  
336 distorted SO<sub>2</sub> enhancement extending above the PBL as determined by the temperature inversion is most likely an artifact of  
337 the saturated sonde, similar to what was seen in the dual-sonde profile from Costa Rica (Fig. 45). As the RH remains low  
338 above the PBL, it is most likely that the SO<sub>2</sub> is contained entirely within the PBL.

## 339 56. Conclusion and Future Work

340 An innovative new method for measuring vertical profiles of SO<sub>2</sub> from TBS and free-release balloons was successfully tested  
341 and demonstrated in controlled laboratory experiments and during four different field deployments covering SO<sub>2</sub>  
342 concentrations ranging from 0.5–325 ppbv during flights and up to 940 ppbv during ground measurements. This new method  
343 requires three major modifications to the standard ECC ozonesonde: the addition of a positive ~~background-bias~~ current in the  
344 cathode cell, an O<sub>3</sub> removal filter, and a sample dryer. Relative to the previous dual-sonde method, the new method measures  
345 SO<sub>2</sub> using a single-sonde system (i.e., the SO<sub>2</sub> sonde). The SO<sub>2</sub> sonde and Thermo 43c-TL measurements were strongly  
346 correlated during laboratory ( $r^2 > 0.99$ ) and field-based ( $r^2 > 0.94$ ) comparisons. Initial field tests and subsequent laboratory  
347 testing of SO<sub>2</sub> sonde v1.0 highlighted the need to dry the sample upstream of the O<sub>3</sub> removal filter to achieve consistent results.  
348 Follow-up field measurements in the Athabasca Oil Sands and Hawai’i clearly demonstrated the improvement in the SO<sub>2</sub> sonde  
349 v1.1’s sensitivity and consistency ( $51 \pm 1.2$  and  $47 \pm 5.8$  ppbv/ $\mu$ A, respectively) as a result of drying the sample.

350  
351 The SO<sub>2</sub> sonde v1.1 offers several advantages over the dual-sonde method, including the ability to measure [SO<sub>2</sub>] independent  
352 of [O<sub>3</sub>], the capability of sub-ppbv detection limits, faster response and recuperation time when exposed to larger SO<sub>2</sub> plumes,  
353 and reduced uncertainty. The lighter weight of the payload requires a smaller balloon and less helium to lift, which may prove  
354 advantageous for deployment under some field conditions, particularly where helium supplies are limited. It’s compactness  
355 and weight can also make it a candidate for ~~small drones and~~ UAV campaigns. Field deployments revealed specific issues and  
356 areas for improvement. The present design requires pre-setting the sonde’s ~~background-bias~~ current prior to the launch. Thus,  
357 some *a priori* estimates of the plume are required to determine the appropriate ~~background-bias~~ current so that the instrument  
358 can measure the full range of SO<sub>2</sub> concentrations present. In the current SO<sub>2</sub> sonde v1.1, increasing the ULOD by applying a  
359 larger ~~background-bias~~ current also increases the LLOD. Further laboratory experiments are needed to identify the factors that

360 cause the remaining observed variability in the SO<sub>2</sub> transmission efficiency in the latest instrument version that includes the  
361 sample dryer. Much of the testing and calibration completed to date assessed the complete SO<sub>2</sub> sonde system (i.e., sonde, filter,  
362 dryer). Building a database of the various individual factors, including pump speeds and filter transmission efficiency, will  
363 [help us to](#) better characterize the causes of sonde-to-sonde variability and allow future versions of the system to improve  
364 performance characteristics so that the system can be made available for operational use. [Additionally, future manuscripts](#)  
365 [topics include intercomparison studies of the SO<sub>2</sub> sonde's vertical profile measurements with other column measurements \(i.e.,](#)  
366 [Pandora\) and satellite measurements and more in-depth analysis of the SO<sub>2</sub> sonde measurements at the various field](#)  
367 [deployments.](#)

Formatted: Font: Not Italic

Formatted: Subscript

#### 368 **Author Contributions**

369 Conceptualization by J.H.F. and G.M. Data curation by J.H.F., A.K., S.L.A., M.G.S., E.K., P.W., G.M., E.C., A.A., and J.A.D.  
370 Formal analysis by A.K., S.L.A., S.Y. and P.W. Funding acquisition by J.H.F. Investigation by A.K., S.L.A., M.G.S., and E.K.  
371 Methodology by J.H.F. and G.M. Writing – original draft preparation by S.Y. Writing – review and editing by P.W. G.M.,  
372 J.A.D. and J.H.F. Supervision by J.H.F.

373 **Conflict of Interest:** The authors declare that they have no conflict of interest.

#### 374 **Acknowledgments**

375 This work was supported by NASA grant numbers NNG11HP16A and 80NSSC18K1061. We especially appreciate our  
376 collaboration with En-Sci in advancing this work. We would also like to thank Mark Gordon of York University and David  
377 Tarasick of Environment Canada for their invitation and assistance with the deployment to Ft. ~~Mackaye~~Murray, to Henry  
378 Selkrik and Holger Vomel from the TicoSonde Project for their support in the Turrialba Volcano testing campaign. A special  
379 thanks to Principal Darlene Javar of Na'alehu Elementary School and its teachers, staff, and students for letting us install  
380 equipment on a roof and helping us with a launch. [Also, we thank the two anonymous reviewers for helpful comments on the](#)  
381 [original draft of this manuscript.](#)

382  
383

**Table 1: Averaged O<sub>3</sub> and SO<sub>2</sub> concentration measured by the SO<sub>2</sub> sonde version 1.0 and Thermo instruments during different stages of testing indicated in Fig. 1.**

	O <sub>3</sub> Thermo (ppbv)	O <sub>3</sub> Sonde (ppbv)	SO <sub>2</sub> Thermo (ppbv)	SO <sub>2</sub> Sonde (ppbv)
A	<del>103-105</del> ± 0.4	100 ± 1.3	<del>-0.3-0</del> ± 0.06	<del>99-96</del> ± 1.83
B	<del>104-105</del> ± 0.5	101.2 ± 0.4	<del>-0.4-0</del> ± 0.06	<del>190-188</del> ± 2.3
C	103 ± 0.4	<del>100-99</del> ± 0.4	57 ± 0.3740	<del>138-135</del> ± 1.0
D	<del>103-105</del> ± 0.55	<del>98-97</del> ± 0.6	116 ± 1.9	<del>81-78</del> ± 1.0
E	-	-	-	-
F	<del>0-131.3</del> ± 0.5	<del>0.53-0.13</del> ± 0.208	116 ± 1.4	<del>5-32.9</del> ± 0.1
G	<del>0-441.1</del> ± 0.4	<del>0-0.51</del> ± 0.11	58 ± 0.7	<del>30-29</del> ± 0.65
H	<del>10-0.61</del> ± 0.439	<del>0.40-15</del> ± 0.0403	24 ± 0.8	<del>67-64</del> ± 0.86
I	<del>0.31-1.3</del> ± 0.2931	<del>10-12-64</del> ± 0.278	-0.25 ± 0.22	<del>91-89</del> ± 0.76

384

385  
386  
387

**Table 2. The SO<sub>2</sub> vertical column density (VCD) for profiles shown in Fig. 7-8 from BISOS in June 2018. For profile c, the descent profile VCD is reported for the flight without extrapolation (shown without parentheses) and using linear extrapolation assuming the SO<sub>2</sub> concentration to be 0 ppbv at sea level (shown in parentheses).**

Profile	Launch Time (UTC)	SO <sub>2</sub> VCD
a (ascent)	06/22/2018 00:32	8.6 DU
b (ascent)	06/28/2018 20:45	12.5 DU
c (descent)	06/29/2018 21:36	6.2 (9.8*) DU
d (ascent)	06/30/2018 20:48	79.1 DU**

\* VCD from extrapolated data

\*\* Saturation of SO<sub>2</sub> at altitudes of 1 to 3 km AMSL

Formatted: Font: Not Bold

Formatted

Formatted: Font: Not Bold

Formatted

Formatted

Formatted: Font: Not Bold

Formatted: Font: Not Bold

Formatted: Font: Not Bold

Formatted: Font: Not Bold

Formatted: Font: Not Bold

Formatted

Formatted: Font: Not Bold

Formatted: Font: Not Bold

Formatted: Font: Not Bold

Formatted

Formatted

Formatted: Font: Not Bold

Formatted

Formatted: Font: Not Bold

Formatted

Formatted

Formatted

Formatted

Formatted

Formatted

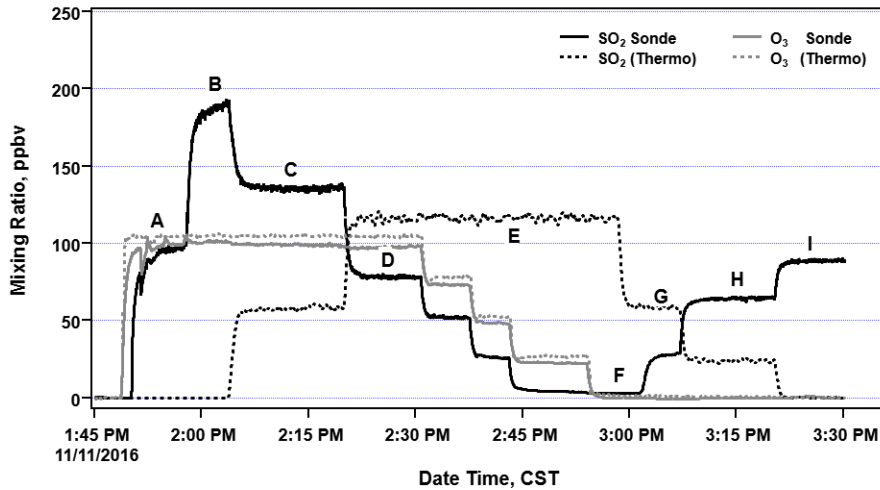
Formatted: Font: Not Bold

Formatted: Centered

Formatted: Centered

Formatted: Centered

Formatted: Centered

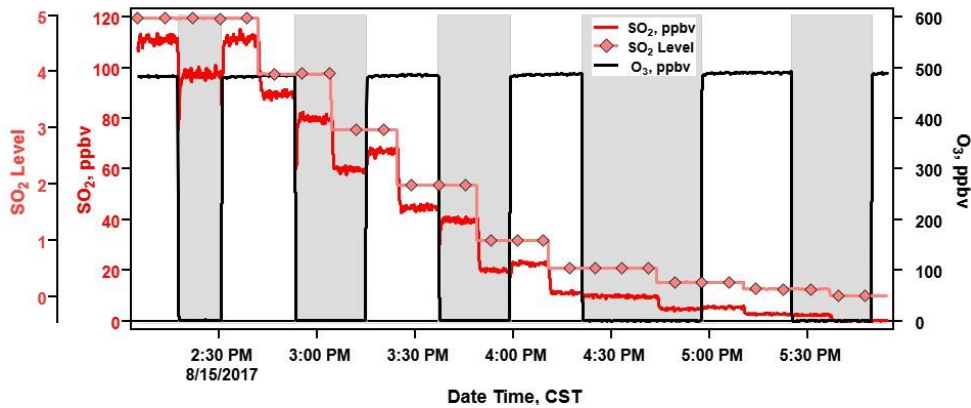


388

389

390

Figure 1: Test of the SO<sub>2</sub> sonde v1.0 (without an O<sub>3</sub> removal filter) with an applied **background bias** current responding to O<sub>3</sub> and SO<sub>2</sub>. See the text for further details.

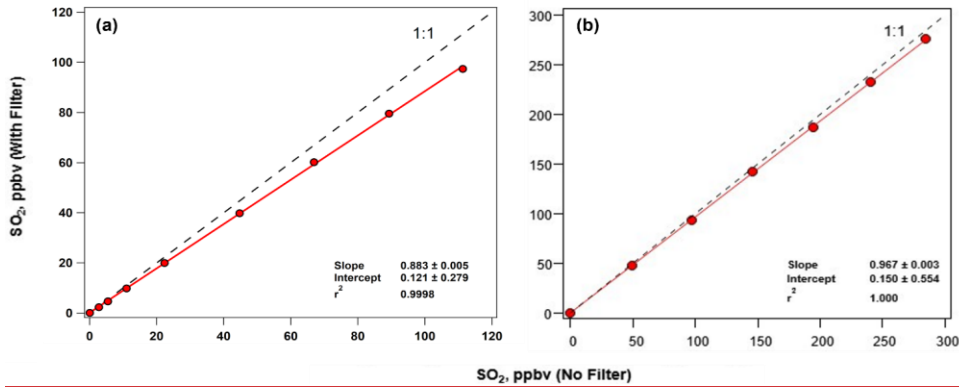


391

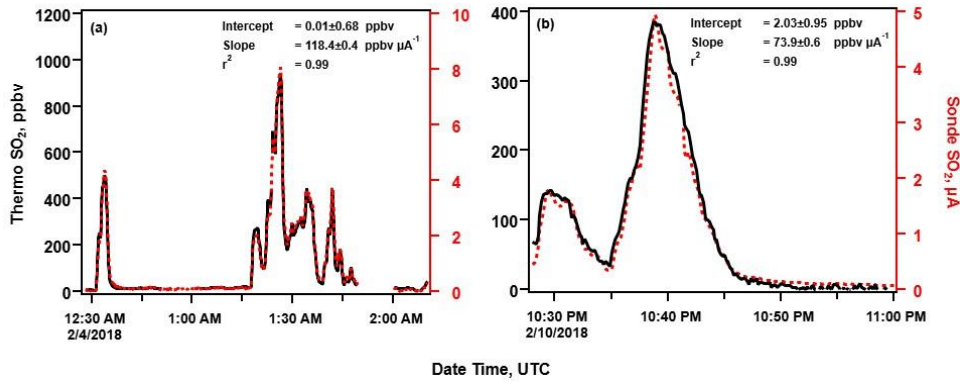
392

393

Figure 2: Time of series of a multipoint test of **the** O<sub>3</sub> filter removal efficiency and impact on SO<sub>2</sub> measurements taken by a Thermo 43i-TL SO<sub>2</sub> analyzer. Changes in SO<sub>2</sub> dilution levels are indicated by the **blue-pink** lines (**diamond markers**).

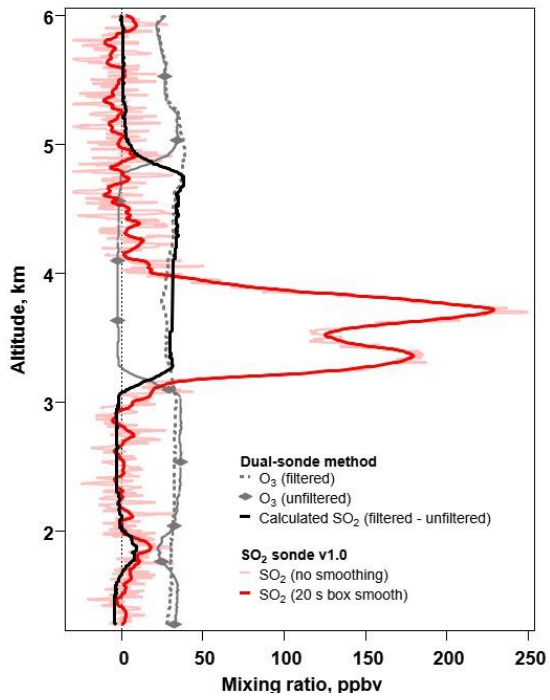


394  
395 **Figure 3:** Response of Thermo 43i-TL SO<sub>2</sub> analyzer with (y-axis) and without (x-axis) an O<sub>3</sub> removal filter using a calibration system  
396 with (a) a processed zero air system and (b) a dry zero air gas cylinder.



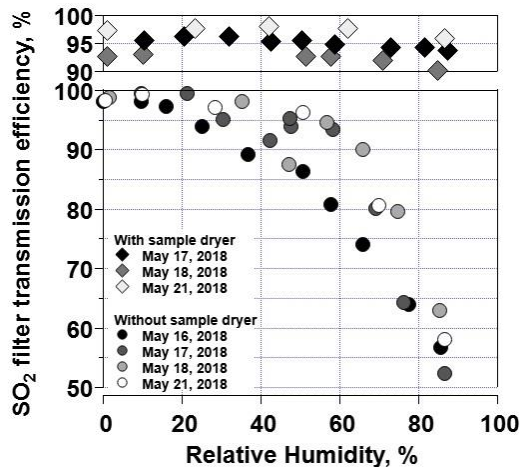
398  
399 **Figure 34:** SO<sub>2</sub> sonde v1.0 and Thermo Environmental SO<sub>2</sub> analyzer measurements at Kilauea, Hawai'i during H3C for (a) initial  
400 SO<sub>2</sub> plume encounter on February 3, 2018, and (b) a pre-flight measurement on February 10, 2018, approximately 6 km downwind  
401 of Kilauea's summit crater.





402  
403  
404

Figure 45: The profiles of a triple-sonde payload, which consisted of a dual-sonde in tandem with an  $SO_2$  sonde v1.0, launched from the Universidad de Costa Rica's campus in San Jose (approximately 31 km downwind of the volcano Turrialba) on March 23, 2018.

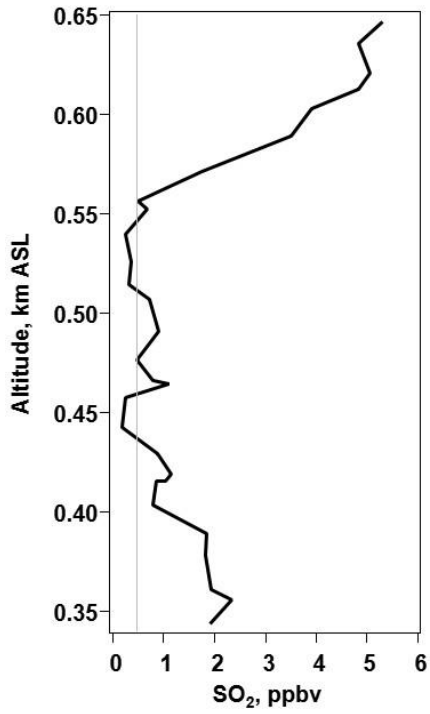


405

406

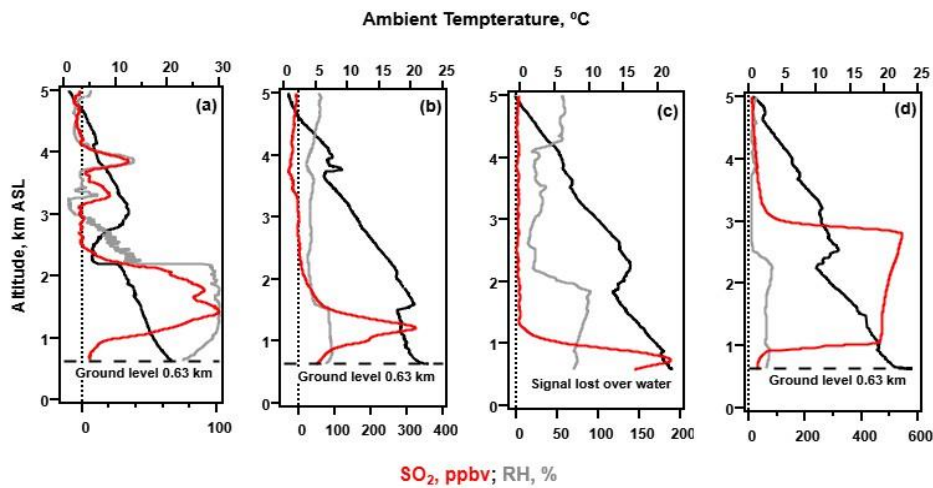
407

Figure 56: Tests of SO<sub>2</sub> transmission efficiency as a function of relative humidity without (circles) and with (diamonds) an upstream sample dryer (diamonds).



408  
409  
410  
411

Figure 67: The profile, constructed using 20 s average changes in altitude (ranging from 1 to 15 km), is for a tethered SO<sub>2</sub> sonde v1.1 in the Athabasca Oil Sands region of Alberta, Canada. The SO<sub>2</sub> sonde background-bias current was 0.5 μA, and the LLOD was 0.47 ppbv.



412

413 **Figure 78:** Vertical profiles of SO<sub>2</sub> (20 s box smoothing) from the SO<sub>2</sub> sonde v1.1 during BISOS in June 2018 with free-release  
 414 balloon launches occurring at the Kahuku Ranch on the Big Island of Hawai'i. Profiles are from (a) 6/22/2018 00:32; (b) 6/28/2018  
 415 20:45; (c) 6/29/2018 21:36; and (d) 6/30/2018 20:48. All times are UTC.

416 **References**

- 417 Anderson, K. R., Johanson, I. A., Patrick, M. R., Gu, M., Segall, P., Poland, M. P., Montgomery-Brown, E. K., and Miklius,  
418 A.: Magma reservoir failure and the onset of caldera collapse at Kīlauea Volcano in 2018, *Science*, 366, 2019.
- 419 Bari, M. A., Kindzierski, W. B., and Roy, P.: Identification of ambient SO<sub>2</sub> sources in industrial areas in the lower Athabasca  
420 oil sands region of Alberta, Canada, *Atmospheric Environment*, 231, 117505, 2020.
- 421 Bluth, G. J., Doiron, S. D., Schnetzler, C. C., Krueger, A. J., and Walter, L. S.: Global tracking of the SO<sub>2</sub> clouds from the  
422 June, 1991 Mount Pinatubo eruptions, *Geophysical Research Letters*, 19, 151–154, 1992.
- 423 Carmichael, G. R. and Peters, L. K.: Some aspects of SO<sub>2</sub> absorption by water-generalized treatment, *Atmospheric*  
424 *Environment* (1967), 13, 1505–1513, 1979.
- 425 Carn, S., Fioletov, V., McLinden, C., Li, C., and Krotkov, N.: A decade of global volcanic SO<sub>2</sub> emissions measured from  
426 space, *Scientific reports*, 7, 1–12, 2017.
- 427 Chen, T.-M., Kuschner, W. G., Gokhale, J., and Shofer, S.: Outdoor air pollution: nitrogen dioxide, sulfur dioxide, and carbon  
428 monoxide health effects, *The American journal of the medical sciences*, 333, 249–256, 2007.
- 429 Delmelle, P., Stix, J., Baxter, P., Garcia-Alvarez, J., and Barquero, J.: Atmospheric dispersion, environmental effects and  
430 potential health hazard associated with the low-altitude gas plume of Masaya volcano, Nicaragua, *Bulletin of Volcanology*,  
431 64, 423–434, 2002.
- 432 Diaz, J. A., Pieri, D., Wright, K., Sorensen, P., Kline-Shoder, R., Arkin, C. R., Fladeland, M., Bland, G., Buongiorno, M. F.,  
433 and Ramirez, C.: Unmanned aerial mass spectrometer systems for in-situ volcanic plume analysis, *Journal of the American*  
434 *Society for Mass Spectrometry*, 26, 292–304, 2015.
- 435 Elias, T., Kern, C., Horton, K. A., Sutton, A. J., and Garbeil, H.: Measuring SO<sub>2</sub> emission rates at Kīlauea Volcano, Hawaii,  
436 using an array of upward-looking UV spectrometers, 2014–2017, *Frontiers in Earth Science*, 6, 214, 2018.
- 437 EPA: National Air Pollutant Emission Trends, 2000.
- 438 Flynn, J. and Morris, G. A.: A method for directly measuring [SO<sub>2</sub>](#) and other trace gases by electrochemical cell ([eeeECC](#))  
439 sonde, [United States Patent 11,150,217](#), 2021.
- 440 Galle, B., Johansson, M., Rivera, C., Zhang, Y., Kihlman, M., Kern, C., Lehmann, T., Platt, U., Arellano, S., and Hidalgo, S.:  
441 Network for Observation of Volcanic and Atmospheric Change (NOVAC)—A global network for volcanic gas monitoring:  
442 Network layout and instrument description, *Journal of Geophysical Research: Atmospheres*, 115, 2010.
- 443 Gansecki, C., Lee, R. L., Shea, T., Lundblad, S. P., Hon, K., and Parcheta, C.: The tangled tale of Kīlauea’s 2018 eruption as  
444 told by geochemical monitoring, *Science*, 366, 2019.
- 445 Kern, C., Sutton, J., Elias, T., Lee, L., Kamibayashi, K., Antolik, L., and Werner, C.: An automated SO<sub>2</sub> camera system for  
446 continuous, real-time monitoring of gas emissions from Kīlauea Volcano’s summit Overlook Crater, *Journal of Volcanology*  
447 *and Geothermal Research*, 300, 81–94, 2015.

448 Kern, C., Lerner, A. H., Elias, T., Nadeau, P. A., Holland, L., Kelly, P. J., Werner, C. A., Clor, L. E., and Cappos, M.:  
449 Quantifying gas emissions associated with the 2018 rift eruption of Kīlauea Volcano using ground-based DOAS  
450 measurements, *Bulletin of Volcanology*, 82, 1–24, 2020.

451 Kiehl, J. and Briegleb, B.: The relative roles of sulfate aerosols and greenhouse gases in climate forcing, *Science*, 260, 311–  
452 314, 1993.

453 Komhyr, W.: Electrical concentration cells for gas analysis, *Ann. Geophys.*, 25, 203–210, 1969.

454 Krug, E. C. and Frink, C. R.: Acid rain on acid soil: a new perspective, *Science*, 221, 520–525, 1983.

455 Liu, T., Chan, A. W., and Abbatt, J. P.: Multiphase Oxidation of Sulfur Dioxide in Aerosol Particles: Implications for Sulfate  
456 Formation in Polluted Environments, *Environmental Science & Technology*, 55, 4227–4242, 2021.

457 McLinden, C. A., Fioletov, V., Krotkov, N. A., Li, C., Boersma, K. F., and Adams, C.: A decade of change in NO<sub>2</sub> and SO<sub>2</sub>  
458 over the Canadian oil sands as seen from space, *Environmental science & technology*, 50, 331–337, 2016.

459 de Moor, J. M., Aiuppa, A., Avarol, G., Wehrmann, H., Dunbar, N., Muller, C., Tamburello, G., Giudice, G., Liuzzo, M., and  
460 Moretti, R.: Turmoil at Turrialba Volcano (Costa Rica): Degassing and eruptive processes inferred from high-frequency gas  
461 monitoring, *Journal of Geophysical Research: Solid Earth*, 121, 5761–5775, 2016.

462 Morris, G. A., Komhyr, W. D., Hirokawa, J., Flynn, J., Lefer, B., Krotkov, N., and Ngan, F.: A balloon sounding technique  
463 for measuring SO<sub>2</sub> plumes, *Journal of Atmospheric and Oceanic Technology*, 27, 1318–1330, 2010.

464 Nadeau, P. A., Werner, C. A., Waite, G. P., Carn, S. A., Brewer, I. D., Elias, T., Sutton, A. J., and Kern, C.: Using SO<sub>2</sub> camera  
465 imagery and seismicity to examine degassing and gas accumulation at Kīlauea Volcano, May 2010, *Journal of Volcanology  
466 and Geothermal Research*, 300, 70–80, 2015.

467 Parker, D. E., Wilson, H., Jones, P. D., Christy, J., and Folland, C. K.: The impact of Mount Pinatubo on world-wide  
468 temperatures, *International Journal of Climatology: A Journal of the Royal Meteorological Society*, 16, 487–497, 1996.

469 Patrick, M., Orr, T., Anderson, K., and Swanson, D.: Eruptions in sync: Improved constraints on Kīlauea Volcano’s hydraulic  
470 connection, *Earth and Planetary Science Letters*, 507, 50–61, 2019.

471 Patrick, M., Johanson, I., Shea, T., and Waite, G.: The historic events at Kīlauea Volcano in 2018: summit collapse, rift zone  
472 eruption, and M w 6.9 earthquake: preface to the special issue, 2020.

473 Pieri, D., Diaz, J. A., Bland, G., Fladeland, M., Madrigal, Y., Corrales, E., Alegria, O., Alan, A., Realmuto, V., and Miles, T.:  
474 In situ observations and sampling of volcanic emissions with NASA and UCR unmanned aircraft, including a case study at  
475 Turrialba Volcano, Costa Rica, *Geological Society, London, Special Publications*, 380, 321–352, 2013.

476 Schmidt, A., Carslaw, K., Mann, G., Wilson, M., Breider, T., Pickering, S., and Thordarson, T.: The impact of the 1783–1784  
477 AD Laki eruption on global aerosol formation processes and cloud condensation nuclei, *Atmospheric Chemistry and Physics*,  
478 10, 6025–6041, 2010.

479 Shannon, J. D.: Regional trends in wet deposition of sulfate in the United States and SO<sub>2</sub> emissions from 1980 through 1995,  
480 *Atmospheric Environment*, 33, 807–816, 1999.

481 Simpson, I., Blake, N., Barletta, B., Diskin, G., Fuelberg, H., Gorham, K., Huey, L., Meinardi, S., Rowland, F., and Vay, S.:  
482 Characterization of trace gases measured over Alberta oil sands mining operations: 76 speciated C<sub>2</sub>–C<sub>10</sub> volatile organic  
483 compounds (VOCs), CO<sub>2</sub>, CH<sub>4</sub>, CO, NO, NO<sub>2</sub>, NO<sub>y</sub>, O<sub>3</sub> and SO<sub>2</sub>, *Atmospheric Chemistry and Physics*, 10, 11931–  
484 11954, 2010.

485 Stein, A.F., Draxler, R.R., Rolph, G.D., Stunder, B.J., Cohen, M.D. and Ngan, F.: NOAA’s HYSPLIT atmospheric transport  
486 and dispersion modeling system, *Bulletin of the American Meteorological Society*, 96(12), 2059–2077, 2015.

487 Sunyer, J., Atkinson, R., Ballester, F., Le Tertre, A., Ayres, J. G., Forastiere, F., Forsberg, B., Vonk, J., Bisanti, L., and  
488 Anderson, R.: Respiratory effects of sulphur dioxide: a hierarchical multicity analysis in the APHEA 2 study, *Occupational  
489 and Environmental Medicine*, 60, e2–e2, 2003.

490 Tang, Y., Tong, D. Q., Yang, K., Lee, P., Baker, B., Crawford, A., Luke, W., Stein, A., Campbell, P. C., and Ring, A.: Air  
491 quality impacts of the 2018 Mt. Kilauea Volcano eruption in Hawaii: A regional chemical transport model study with satellite-  
492 constrained emissions, *Atmospheric Environment*, 237, 117648, 2020.

493 Terraglio, F. P. and Manganelli, R. M.: The absorption of atmospheric sulfur dioxide by water solutions, *Journal of the Air  
494 Pollution Control Association*, 17, 403–406, 1967.

495 Tortini, R., van Manen, S., Parkes, B., and Carn, S.: The impact of persistent volcanic degassing on vegetation: A case study  
496 at Turrialba volcano, Costa Rica, *International journal of applied earth observation and geoinformation*, 59, 92–103, 2017.

497 Tzortziou, M., Herman, J. R., Cede, A., Loughner, C. P., Abuhassan, N., and Naik, S.: Spatial and temporal variability of  
498 ozone and nitrogen dioxide over a major urban estuarine ecosystem, *Journal of Atmospheric Chemistry*, 72, 287–309, 2015.

499 Tzortziou, M., Parker, O., Lamb, B., Herman, J. R., Lamsal, L., Stauffer, R., and Abuhassan, N.: Atmospheric Trace Gas (NO<sub>2</sub>  
500 and O<sub>3</sub>) variability in South Korean coastal waters, and implications for remote sensing of coastal ocean color dynamics,  
501 *Remote Sensing*, 10, 1587, 2018.

502 Xi, X., Johnson, M. S., Jeong, S., Fladeland, M., Pieri, D., Diaz, J. A., and Bland, G. L.: Constraining the sulfur dioxide  
503 degassing flux from Turrialba volcano, Costa Rica using unmanned aerial system measurements, *Journal of Volcanology and  
504 Geothermal Research*, 325, 110–118, 2016.

505 Zhang, Q., Tie, X., Lin, W., Cao, J., Quan, J., Ran, L., and Xu, W.: Variability of SO<sub>2</sub> in an intensive fog in North China Plain:  
506 Evidence of high solubility of SO<sub>2</sub>, *Particuology*, 11, 41–47, 2013.

507 Zhang, R., Wang, G., Guo, S., Zamora, M. L., Ying, Q., Lin, Y., Wang, W., Hu, M., and Wang, Y.: Formation of urban fine  
508 particulate matter, *Chemical reviews*, 115, 3803–3855, 2015.

509 Zhang, X. and Schreifels, J.: Continuous emission monitoring systems at power plants in China: Improving SO<sub>2</sub> emission  
510 measurement, *Energy Policy*, 39, 7432–7438, 2011.

511

**Formatted:** Font: (Default) Times New Roman

**Formatted:** Font: (Default) Times New Roman

**Formatted:** Font: (Default) Times New Roman

**Formatted:** Font: (Default) Times New Roman, Not  
Italic

**Formatted:** Font: (Default) Times New Roman

**Formatted:** Font: (Default) Times New Roman, Not  
Italic

**Formatted:** Font: (Default) Times New Roman

**Formatted:** Font: (Default) Times New Roman